

# High-order LES modeling of turbulent incompressible flow

R. Pasquetti <sup>a</sup>

<sup>a</sup> Lab. J.A. Dieudonné, UMR CNRS 6621,  
Université de Nice-Sophia Antipolis, Nice, France  
E-mail: Richard.Pasquetti@unice.fr

(Reçu le jour mois année, accepté après révision le jour mois année)

---

**Abstract.** The paper presents the high-order algorithms that we have developed for the large-eddy simulation of incompressible flows and the results that have been obtained for the 3D turbulent wake of a cylinder at a Reynolds number of  $Re = 3900$ . © 2001 Académie des sciences/Éditions scientifiques et médicales Elsevier SAS

**Large-eddy simulation/ Spectral methods/ Wake flows/**

*Simulation des grandes échelles d'écoulements incompressibles turbulents par méthode d'ordre élevé*

**Résumé.** *l'article présente les algorithmes d'ordre élevé que nous avons développés pour la simulation des grandes échelles d'écoulements incompressibles ainsi que les résultats obtenus pour le sillage 3D turbulent d'un cylindre à un nombre de Reynolds de  $Re = 3900$ . © 2001 Académie des sciences/Éditions scientifiques et médicales Elsevier SAS*

*Simulation des grandes échelles/ Méthodes spectrales/ Ecoulements de type sillage/*

---

## 1. Introduction

Despite the amazing increase of the computer capacities and the efforts made to elaborate a complete theory of turbulence, the direct numerical simulation (DNS) and the statistical approaches, based on the Reynolds Averaged Navier-Stokes (RANS) equations, do not yet permit satisfactory computations of turbulent complex flows. Between DNS and RANS stands the large-eddy simulation (LES) approach, based on the idea of computing only the large eddies of the flow and to restrict the modeling to the smaller ones. This approach remains, and probably for some times, adequate to compute turbulent flows. However, in order to clearly discern the numerical approximation errors and the sub-grid-scale (SGS) modeling, using high-order methods is from our point of view a fundamental requirement, especially to deal with some detailed studies of fluid dynamics.

---

Note présentée par First name NAME

S1620-7742(01)0????-?/FLA

© 2001 Académie des sciences/Éditions scientifiques et médicales Elsevier SAS. Tous droits réservés.

To compute 3D wakes in channel-like geometries with a homogeneous spanwise direction, we use a multi-domain Chebyshev-Fourier spectral approximation in space and a second order semi-Lagrangian projection method in time. The SGS model makes use of the so-called approximate deconvolution method (ADM) [10, 22], which may be viewed as an extension of the scale similarity model [2]. In the frame of our numerical scheme then arise the Defiltering-Transport-Filtering (DTF) algorithms that we introduced in [19]. SGS models based on scale similarity are known to be better on a priori tests than those based on an eddy-viscosity, typically the Smagorinsky model (see e.g. [21]), possibly associated with the dynamic modeling [9]. However, they are also known to yield numerical instabilities, which may be overcome by combining in more or less empirical ways the scale similarity and eddy-viscosity concepts [6]. The approach that we propose is to use the DTF modeling combined with the spectral vanishing viscosity (SVV) method to stabilize the calculations. The SVV method, first developed to solve non-linear hyperbolic equations, typically the Burgers equation, with the Fourier [24] or Legendre [17] spectral method, shows indeed the property to preserve the spectral accuracy of the approximation. Thus, the convergence of the numerical approximation toward the exact solution remains exponential, even of course if the convergence rate is worse with a SVV term than without. Note that the present approach should not be confused with those making use of a spectral viscosity, on the grounds of homogeneous and isotropic turbulence theory [16]).

After a the description, in Section 2, of the high-order scheme and of the associated LES modeling of turbulent inhomogeneous flows we present, in Section 3, the results that we have obtained for a classical benchmark: the turbulent wake of a cylinder, the Reynolds number being equal to  $Re = 3900$ . Especially we compare results obtained when using DTF, for the SGS modeling, stabilized with SVV with the no-SGS model approach making only use of SVV. We discuss these results in Section 4 and finally conclude in Section 5.

## 2. The spectral LES model

Along the streamwise direction we use a domain decomposition technique to efficiently handle the elongated geometries typically encountered when studying wake type flows. In each subdomain we use spectrally accurate approximations, based on Chebyshev polynomials in the  $x$ -streamwise and  $y$ -cross-flow directions and on Fourier series in the  $z$ -spanwise homogeneous direction. The time-scheme makes use of 3 steps: a transport step, to handle the convective term, a diffusion term, to handle the viscous term and a projection step, to finally obtain a divergence-free velocity field. The LES modeling, i.e. the DTF algorithm, is implemented in the transport step and the SVV stabilization technique in the diffusion step.

To model the bluff body, inside the channel, we use a smoothed penalty technique. Essentially, the smoothing is realized through a filtering of its characteristic function, like in [8], but now we use for the filtering an improved version of the "raised cosine filter" in order to more precisely take into account the position of the bluff body. Such a modeling implies that spectral accuracy is lost, at least locally. Here we assume that the phenomenon remains local and thus does not drastically affect the flow, especially the far wake.

The equations that we have to solve are then the filtered Navier-Stokes equations with a body force term to model the bluff body. Denoting, as it is usual (see e.g. [21]), with an over bar the filtered quantities we assume that the large scales of the (incompressible) flow are governed by the dimensionless equations:

$$\overline{D_t \mathbf{u}} = -\nabla \bar{p} + \frac{1}{Re} \nabla^2 \bar{\mathbf{u}} + \bar{\mathbf{f}} \quad (1)$$

$$\nabla \cdot \bar{\mathbf{u}} = 0 \quad (2)$$

with  $D_t$  the material derivative and  $t$  the time,  $\mathbf{u}$  the velocity field,  $p$  the pressure,  $\mathbf{f}$  a force term and  $Re$  the Reynolds number.

Let us now describe briefly the different steps of the algorithm together with the implementation of the LES modeling (more details may be found in [4]). For the sake of simplicity in the notations but also to

clearly outline that the diffusion and projection steps are similar to those of the DNS implementation, we omit the over bars in their descriptions.

**Transport step and DTF algorithm:** The approximation of the material derivative with a BEQ (backward Euler of order  $Q$ ) scheme yields, with  $\alpha_q, q = 0, \dots, Q$  a set of given coefficients:

$$D_t \mathbf{u}(t_{n+1}) = \frac{1}{\Delta t} (\alpha_0 \mathbf{u}^{n+1} + \sum_{q=1}^{q=Q} \alpha_q \tilde{\mathbf{u}}^{n+1-q}) + O(\Delta t^Q)$$

with  $\mathbf{u}^{n+1} \approx \mathbf{u}(\mathbf{x}, t_{n+1})$  and  $\tilde{\mathbf{u}}^{n+1-q} \approx \mathbf{u}(\chi(\mathbf{x}, t_{n+1}; t_{n+1-q}), t_{n+1-q})$ , where  $\chi(\mathbf{x}, t_{n+1}; t)$  solves the characteristics equation stemming from  $(\mathbf{x}, t_{n+1})$ . To compute the  $\tilde{\mathbf{u}}^{n+1-q}$ , the natural approach is then to determine for each mesh-point  $\mathbf{x}_k$  the value of the velocity  $\mathbf{u}$  at the times  $\{t_n, t_{n-1}, \dots, t_{n+1-Q}\}$  and at the points  $\chi(\mathbf{x}_k, t_{n+1}; t_{n+1-q})$ ,  $q = 1, \dots, Q$ . However, the ‘‘method of characteristics’’ cannot be used in the frame of standard spectral methods because high-order interpolations would be too expensive and moreover would yield numerical instabilities. To overcome this difficulty we use an ‘‘Operator Integration Factor’’ (OIF) Semi-Lagrangian method [18, 20, 25]. The basic idea is here to transport the  $\mathbf{u}^{n+1-q}(\chi(\mathbf{x}_k, t_{n+1}; t_{n+1-q}))$  at the mesh points, so that interpolations / extrapolations are only needed in time. This requires to solve, with in our case the RK4 (fourth order Runge Kutta) scheme and possibly sub-time cycling, a set of  $Q$  problems involving an advection equation (for details see [4]).

Applying now the filtering operator we get:

$$\overline{D_t \mathbf{u}} \approx \frac{1}{\Delta t} (\alpha_0 \bar{\mathbf{u}}^{n+1} + \sum_{q=1}^{q=Q} \alpha_q \bar{\tilde{\mathbf{u}}}^{n+1-q})$$

Then the closure problem consists in determining the  $\bar{\tilde{\mathbf{u}}}^{n+1-q}$  from the  $\bar{\mathbf{u}}^{n+1-q}$ . To do that, we use an ADM type approach, i.e. we introduce an approximate inverse of the filtering operator. The algorithm proposed in [19, 4] reads:

$$\bar{\tilde{\mathbf{u}}}^{n+1-q} = (1 + G(T - 1)G^+) \bar{\mathbf{u}}^{n+1-q}$$

where  $G$  denotes the filtering operator,  $G^+$  the approximate inverse of  $G$  and  $T(\mathbf{u})$  the transport operator such that  $\tilde{\mathbf{u}}^{n+1-q} = T\mathbf{u}^{n+1-q}$ . Let us remark that the straightforward approach,  $\bar{\tilde{\mathbf{u}}}^{n+1-q} = GTG^+ \bar{\mathbf{u}}^{n+1-q}$ , yields a non-consistent algorithm. Indeed, in the limit  $\Delta t = 0$ , for which  $T = 1$ , we have  $GG^+ \neq 1$ . The choice of the operators  $G$  and  $G^+$  is of course crucial. In the frame of a Fourier-Chebyshev spectral method it of interest to apply the filtering operations in Fourier space, where the convolution products resumes to simple products. In fact we use for  $G$  and  $G^+$  quadratic approximations of the Gaussian filter and of its inverse, as shown in Fig. 1, but in order to avoid the meaningless negative values of the  $G$ -spectrum, we cancel them in the higher wave number range ( $G'$ -spectrum).

**Diffusion step and SVV stabilization:** In the diffusion step one computes a provisional velocity such that:

$$\left( \frac{1}{Re} \nabla^2 + S - \frac{\alpha_0}{\Delta t} \right) \mathbf{u}^* = \mathbf{s}^{n+1} \quad \text{in } \Omega \quad (3)$$

$$+B.C., \quad e.g. \quad \mathbf{u}^*|_{\Gamma} = \mathbf{u}^{n+1}|_{\Gamma} = \mathbf{u}_{\Gamma} \quad (4)$$

where  $S$  is the SVV stabilization operator and where:

$$\mathbf{s}^{n+1} = \frac{1}{\Delta t} \sum_{q=1}^{q=Q} \alpha_q \tilde{\mathbf{u}}^{n+1-q} + \nabla p^* - \mathbf{f}^{n+1}$$

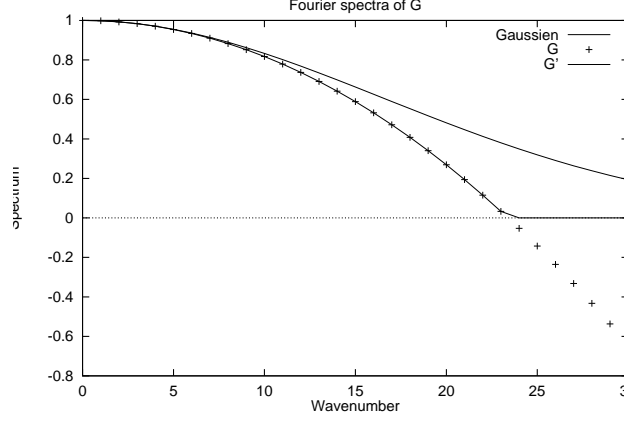


Figure 1: Spectra of the Gaussian filter and of its approximations  $G$  and  $G'$ . The (non-plotted) spectrum of  $G^+$  is symmetric to the one of  $G$

with  $p^*$  a provisional pressure. In the frame of a second order implementation:  $Q = 2$  and  $p^* = p^n$  (“Goda scheme” [11]).

Our definition of the SVV operator  $S$  relies on the one introduced in [17] for the resolution, in the interval  $(-1, 1)$ , of 1D hyperbolic equations by using the spectral Legendre method. In this case, with  $P_N(-1, 1)$  the space of polynomials of maximum degree  $N$ , we have:

$$S u := \epsilon_N \partial_x Q(\partial_x u)$$

where  $Q$  is the operator such that, with  $L_k$  the Legendre polynomial of degree  $k$ :

$$Q\phi \equiv \sum_{k=0}^N \hat{Q}_k \hat{\phi}_k L_k, \quad \forall \phi, \quad \phi = \sum_{k=0}^N \hat{\phi}_k L_k$$

with  $\epsilon_N = O(N^{-1})$ ,  $\hat{Q}_k = 0$  if  $k \leq m_N$  and  $1 \geq \hat{Q}_k > 0$  if  $k > m_N$ . Typical choices for  $m_N$  are  $m_N = O(\sqrt{N})$  [17] or  $m_N = N/2$  [14]. For  $m_N < k \leq N$  the numerical experiments show that a smooth variation for  $\hat{Q}_k$  yields better results. Thus, as in [17] we will use:

$$\hat{Q}_k = \exp\left(-\left(\frac{N-k}{m_N-k}\right)^2\right), \quad k > m_N.$$

In our multidimensional framework such a SVV term may be extended in:

$$S u_i^* := \epsilon_N \nabla \cdot Q(\nabla u_i^*)$$

with  $u_i^*$  any component of  $\mathbf{u}^*$  and where  $Q$  applies independently to each component of  $\nabla u_i^*$ . Let us remark that such an extension of the initial 1D definition may be discussed, especially when complex geometries are considered [26]. Let us also mention that with  $L$  a characteristic dimensionless length of the computational domain (subdomain in our case) then, from scaling arguments,  $\epsilon_N = O(L/(2N))$ .

**Projection step:** To derive from  $\mathbf{u}^*$  a divergence-free velocity field  $\mathbf{u}$ , we solve the *Darcy problem*:

$$\begin{aligned} \mathbf{u}^{n+1} + \nabla \varphi &= \mathbf{u}^* \quad \text{in } \Omega \\ \nabla \cdot \mathbf{u}^{n+1} &= 0 \quad \text{in } \Omega \\ \mathbf{u}^{n+1} \cdot \mathbf{n}|_{\Gamma} &= \mathbf{u}_{\Gamma} \cdot \mathbf{n} \end{aligned}$$

and then update the pressure field  $p^{n+1} = p^n + \alpha_0 \varphi / \Delta t$ .

Solving the above Darcy problem is not straightforward. Following [1, 3] we use a *unique grid*  $P_N - P_{N-2}$  strategy. Essentially, this means that the polynomial spaces of the pressure and of the velocity components are chosen different, so that no boundary conditions are required for the pressure which is completely defined by its values at the inner grid-points. Thus, in the monodomain case the polynomial interpolant of the pressure is 2 degrees less than for the velocity components in the non-homogeneous directions. Some details on the multidomain case are given in [4].

### 3. Turbulent wake of a cylinder ( $Re = 3900$ )

As e.g. in [15] we are interested in the computation of the turbulent wake of a cylinder at a Reynolds number (based on the diameter and on the mean flow velocity) of  $Re = 3900$ . Moreover, the Navier-Stokes equations are solved together with a transport-diffusion equation for the temperature, without coupling, i.e. the temperature behaves as a passive scalar.

With  $x, y, z$  for the longitudinal, cross-flow and spanwise directions, respectively, the computational domain is  $\Omega = (-6.5, 17.5) \times (-4, 4) \times (0, 4)$ , and the cylinder is of unit diameter with axis at  $x = y = 0$ .

The initial and boundary conditions are, in dimensionless form: (i) at  $t = 0$ , fluid at rest ( $\mathbf{u}(t = 0) = 0$ ) and thermally stratified ( $T(t = 0) = y$ ) and (ii) Dirichlet conditions at the inlet ( $\mathbf{u}(x = -6.5) = 1$ ,  $T(x = 0) = y$ ), free-slip conditions for  $\mathbf{u}$  and adiabaticity conditions for  $T$  at the horizontal boundaries ( $y = \pm 4$ ), soft outflow boundary conditions (see [8]) at the outlet ( $x = 17.5$ ).

The calculations have been carried out with the following spatial approximation: number of subdomains in  $x$ -direction  $S = 5$ , Chebyshev polynomial degree in  $x$  and  $y$ ,  $N_1 = 60$  and  $N_2 = 120$  respectively, number of Fourier-grid points in  $z$ ,  $N_F = 60$ . We have used a time-step  $\Delta t = 5 \cdot 10^{-3}$  without sub-cycling in the transport step. For the SVV parameters we chose  $\epsilon_N = 1/N$  and  $m_N = \sqrt{N}$ . Visualizations at

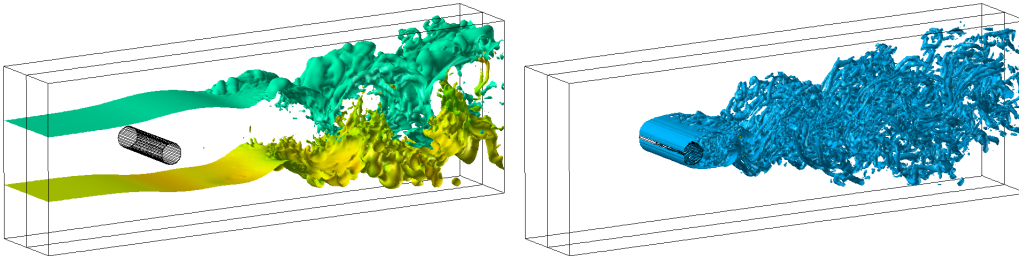


Figure 2: Isotherms (left) and Q criterion (right) with SVV

a given time of the 3D flow computed with the SVV method are shown in Fig. 2. At left the isotherms  $T = \pm 1.5$  are visualized and at right it is the  $Q$  criterion (see e.g. [13]). The streamwise and spanwise components of the vorticity, as computed with the SVV method, are shown in Fig. 3. Quite similar results

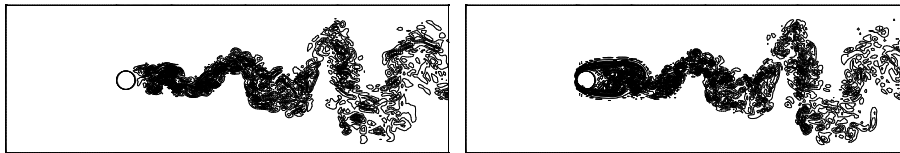


Figure 3: Streamwise (left) and spanwise (right) components of the vorticity with SVV

are obtained when using the DTF algorithm associated to the SVV method for stabilization (see [4] for such

qualitative comparisons). In Fig. 4 the time variations of the temperature at two “boundary points” of the wake, as computed with the SVV and DTF algorithms, are presented. Large departure of the temperature may be observed, corresponding to the crossing of some larger eddies at these specific points. Hereafter we

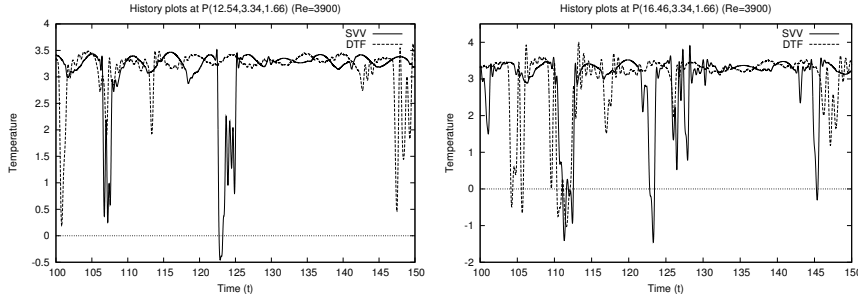


Figure 4:  $T(t)$  for DTF and SVV;  $P = (12.54, 3.34, 1.66)$  (left),  $P = (16.46, 3.34, 1.66)$  (right)

present more quantitative results. First we examine mean velocity profiles and second the power spectra obtained from the evolutions of the velocity components at some particular points of the flow. The results are given for computations made with the SVV stabilization technique, with the DTF-SVV algorithm and also with the SVV method when adding some noise at the inlet (“SVV+noise”). To this end, a white noise of amplitude 0.005 is added to the  $y$  and  $z$  components of the inflow velocity. Our goal is both to check the validity of our calculations and to provide detailed comparisons of the SVV, DTF-SVV and SVV+noise results.

### 3.1. Mean profiles

The mean profiles have been computed from time  $t = 75$ , at which the turbulent flow may be considered as established, to time  $t = 150$ , i.e. on a time interval corresponding approximatively to 7.5 shedding periods. Fig. 5 shows the variation of the velocity mean streamwise component along the  $x$ -axis. The right part

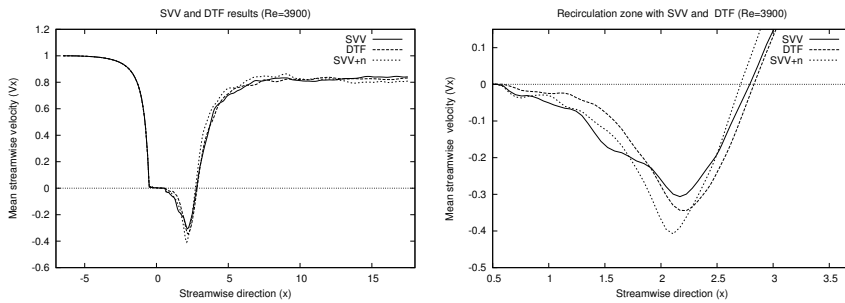


Figure 5:  $\bar{u}_x(x)$ , along  $y = z = 0$  (DTF, SVV and SVV+n)

of the figure gives a zoom of the recirculation zone. First it should be mentioned that this recirculation zone appears longer than the one observed in the experiments or in other computations [15, 12]. From our point of view, this may directly result from the fact that the height of our computational domain only equals 8, which is not enough to make comparisons with results obtained in an open (or quasi-open) domain. However, one remarks from [15, 12] that higher order methods seem to yield a longer recirculation zone. Second, one observes that the discrepancies between our three computations, SVV, DTF-SVV and SVV+noise are not important. Thus, the DTF result lies approximatively between those of SVV and SVV+noise. Mean

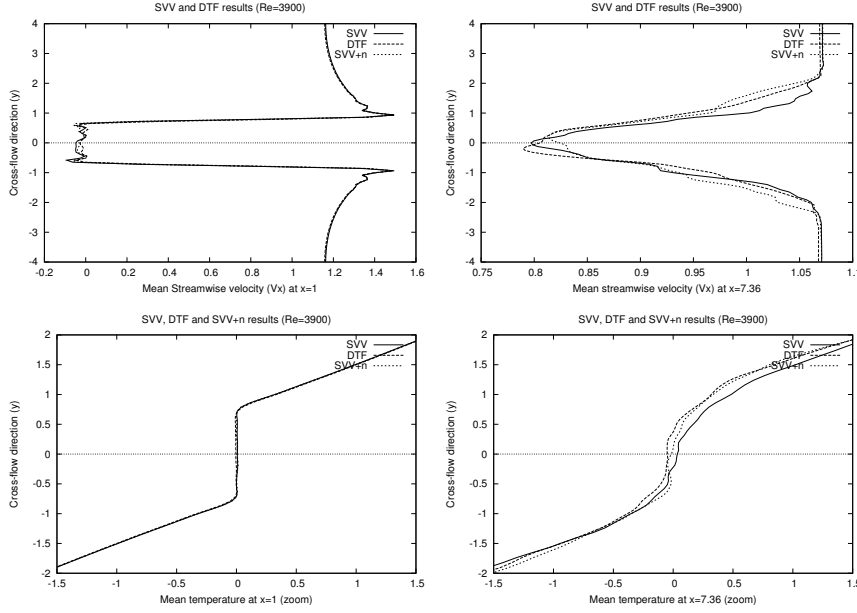


Figure 6:  $\bar{u}_x(y)$  (top) and  $\bar{T}(y)$  (bottom) for  $x = 1$  and  $x = 7.36$  ( $z = 0$ ) (DTF, SVV and SVV+n)

streamwise velocity profiles are shown in Fig. 6. The left one is located in the recirculation zone, and the right one downflow. Zooms of the corresponding temperature profiles are also shown in Fig. 6. Here again one observes that the three computations yield similar results, especially close to the cylinder. Downflow, one may assume that the small discrepancies that can be observed essentially result from a not enough long averaging time, as pointed out by some lack of symmetry of the profiles.

### 3.2. Power spectra

In order to go into the details of the LES modeling, one has to analyze the frequency content of the velocity field. For inhomogeneous flows, it is convenient to proceed as in experiments, from time evolutions of the velocity components at different points. Through the Taylor hypothesis one can then produce power spectra representative of the distribution of the turbulent kinetic energy in wavenumber space, and then compare it to the Kolmogorov law describing the inertial range. This gives again a way to compare the results obtained with the SVV, DTF-SVV and SVV+noise computations. In Fig. 7 are compared the time variations at a given point of the  $x$  and  $y$ -components of the velocity, computed with SVV and DTF-SVV. The corresponding power spectra are also presented and compared with the  $k^{-5/3}$  slope of the Kolmogorov theory. Essentially one observes that the dimensionless shedding frequency (the Strouhal number) approximately equals 0.2 and that the power spectra show the expected behavior in one part of the spectrum, before decreasing faster in a numerical dissipation frequency range. Also, one clearly observes that this dissipation range is slightly larger for the DTF-SVV than for the SVV computations. The filtering part of the DTF algorithm is certainly responsible for this behavior.

Power spectra obtained for SVV and SVV+noise are plotted in Fig. 8. This figure also shows the power spectra obtained for the  $z$ -component of the velocity, using SVV, SVV-DTF and SVV+noise. One observes similar results for this component of the velocity, except maybe that the inertial range appears to be a little bit smaller.

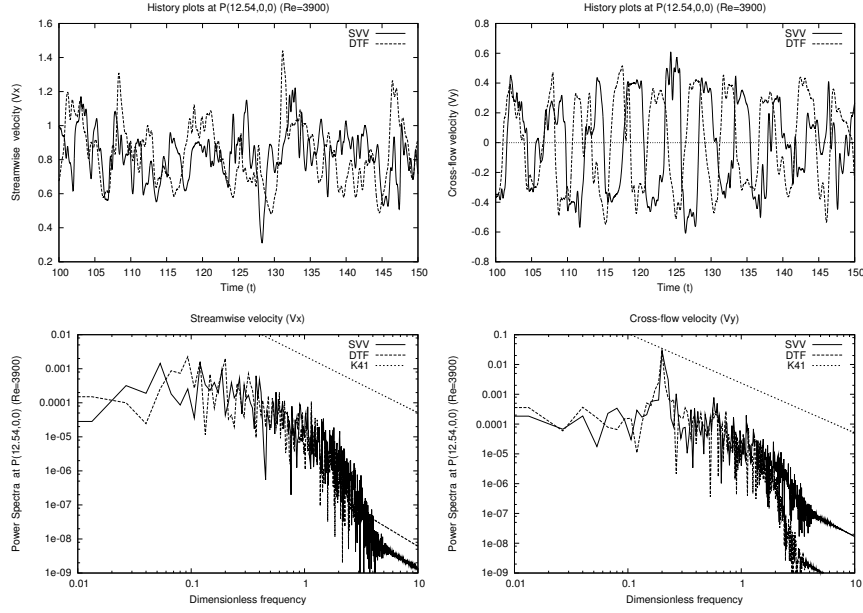


Figure 7:  $u_x(t)$  (left),  $u_y(t)$  (right) and corresponding spectra for DTF and SVV;  $P = (12.54, 0, 0)$

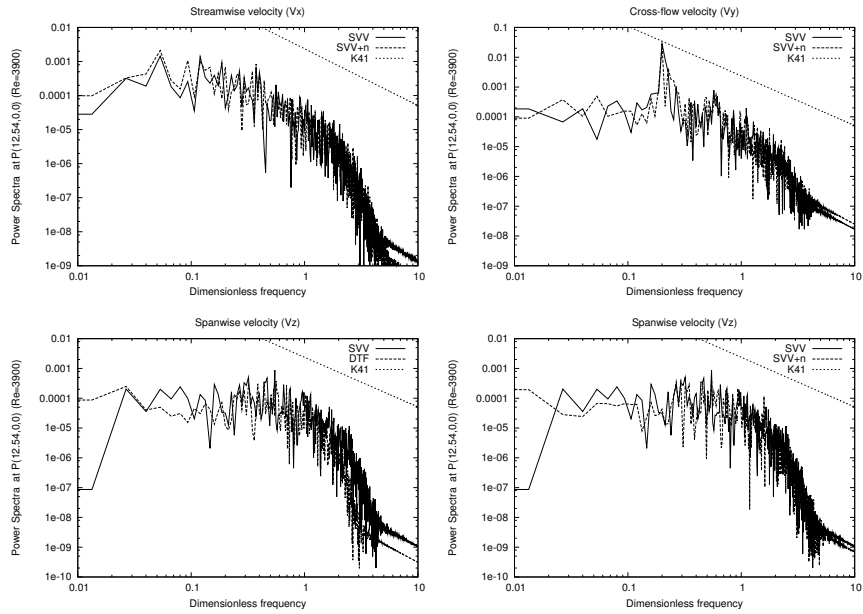


Figure 8: Top:  $u_x$  (left) and  $u_y$  (right) power spectra for SVV and SVV+noise;  $P = (12.54, 0, 0)$  ; Bottom:  $u_z$  power spectra for SVV and DTF (left) and for SVV and SVV+noise (right);  $P = (12.54, 0, 0)$

#### 4. Comments

The striking point of the present study is that the no-model approach, making only use of the stabilization technique, and the ADM type DTF modeling have yielded very similar results. This may be due to the choice of the SVV tuning parameters,  $\epsilon_N$  and  $m_N$ . Especially, the SVV activation parameter  $m_N$  was chosen small ( $m_N = \sqrt{N}$ ). It remains that the no-model approach has yielded satisfactory results, especially when looking at the power-spectra. Even more, in the high frequency range, the no-model approach appears better than the DTF one.

Nevertheless it is expected that taking into account the sub-grid scales contributions of the flow improves the LES modeling. In the frame of ADM approaches, the choice of the filtering and defiltering operators may be important. Especially, our conviction is that the ADM can only result in some non-controlled noise for the SGS model contribution if it is not associated with a two-level grid approach, (see e.g. [5]). Thus, for the DTF algorithm, one may think as necessary to represent the defiltered quantities on a finer grid than the filtered ones. In this spirit, using the filter  $G'$  (see Fig. 1), whose spectrum vanishes beyond a critical wavenumber, say  $k_c$ , is from our point of view fully justified. Using such a filter is clearly close to using a two-level grid technique, with the advantage of the higher flexibility offered by the fact of working in spectral space than working in physical space. Thus, for fully periodic problems, the filtered quantities would not show spatial frequencies beyond  $k_c$ , and it is only during the transport step, in which the non-linear convective term is taken into account, that the full frequency range would be used to handle the defiltered quantities. In the frame of a two-level grid approach, the high wave-number range should be disregarded, since we are only interested in the computation of the filtered quantities. As a result, the fact that with the DTF method the power spectra are slightly worse in the high frequency range than with the no-model approach should also be disregarded. But it remains that our present choice of the filtering and defiltering operators can certainly be improved.

Our LES modeling is fully explicit, in the sense that the filtering (and defiltering) operation is explicitly applied. To this end, we work in spectral space, both for the Fourier and for the Chebyshev approximations. In case of the Chebyshev approximation this corresponds to apply a filter of constant width to the  $2\pi$ -periodic function  $u(-\cos(z))$ ,  $z \in R$ , i.e. to first map the Gauss-Lobatto-Chebyshev grid to a regular grid and then to extend it, first by symmetry and then by periodicity. This procedure is close to the one suggested in [7], where the filtering operation in case of non-equidistant grid-points is defined by a mapping from the computational domain to the real axis. Moreover, such a procedure may be extended to meshes different of the Chebyshev-Gauss-Lobatto mesh, as soon as it exists a smooth even and  $2\pi$ -periodic mapping to similarly associate a Fourier type grid to the computational grid (1D case).

#### 5. Conclusion

Two variants of a high-order LES model have been described and then compared by computing the wake of a cylinder at Reynolds number  $Re = 3900$ . The first one makes only use of the SVV stabilization technique, which shows the essential property to preserve the exponential convergence of the spectral approximation. This approach may be classified as a no-model approach, in the sense that modeling the SGS tensor is not attempted. On the contrary the second one combines an ADM type approach (the DTF algorithm in the frame of our semi-Lagrangian method) and the SVV stabilization technique. Both quantitatively and qualitatively, satisfactory and very similar results have been obtained. Especially, the power spectra show a behavior in agreement with Kolmogorov theory in a large wavenumber range.

**Acknowledgements.** The computations were made on the NEC-SX5 computer of the IDRIS computational center (project 024055). We are grateful to J.M. Lacroix, engineer of the CNRS, for his helpful contribution, especially for the fluid flow visualizations.

## References

- [1] Azaiez, M. et al. (1994). A unique grid spectral solver of the  $nD$  Cartesian unsteady Stokes system. Illustrative numerical results, *Finite Elem. Anal. Des.*, **16**, (3-4), 247-260.
- [2] Bardina, J. et al. (1983). Improved turbulence models based on large eddy simulation of homogeneous incompressible turbulence, Stanford University, Report TF-19.
- [3] Botella, O. (1997). On the solution of the Navier-Stokes equations using Chebyshev projection schemas with third order accuracy in time. *Computers & Fluids*, **26** (2), 107-116.
- [4] Cousin, L. and Pasquetti, R. (2003). High-order methods for the simulation of transitional to turbulent wakes, *third Int. Workshop on Scientific Computing and Applications*, City University Hong-Kong, 6-9 January 2003.
- [5] Domaradzki, J.A. and Saiki, E.M. (1997). A subgrid-scale model based on the estimation of unresolved scales of turbulence, *Phys. Fluids*, **9**(7), 2148-2164.
- [6] Gatsky, T.B., Hussaini, M.Y. and Lumley, J.L. (1996). Simulation and modeling of turbulent flows, *ICASE/LaRC Series in Computational Science and Engineering*, Chapter 3, Large Eddy Simulation, by J.H. Ferziger, pp. 109-154.
- [7] Ghosal, S. and Moin, P. (1995). The basic equations for the large-eddy simulation of turbulent flows in complex geometry, *J. Comput. Phys.*, **118**, 24-37.
- [8] Forestier, M.Y. et al. (2000). Computations of 3D wakes in stratified fluids, *Computational Fluid Dynamics Conference ECCOMAS 2000*, proc. in CD.
- [9] Germano, M. et al. (1991). A dynamic sub-grid scale eddy viscosity model. *Phys. Fluids*, **3** (7), 1760-1765.
- [10] Geurt, B.J. (1997). Inverse modeling for large-eddy simulation, *Phys. Fluids*, **9**(12), 3585-3587.
- [11] Goda, K. (1979). Inverse modeling for large-eddy simulation, A multistep technique with implicit difference schemes for calculation two and three dimensional cavity flows. *J. Comput. Phys.*, **30**(12), 76-95.
- [12] Hansen, R.P. and Long, L.N. (2002). Large-eddy simulation of a circular cylinder on unstructured grids. *Proc. of 40th AIAA Aerospace Sciences Meeting and Exhibit*, 14-17 January 2002.
- [13] Jeong, J. and Hussain (1995). On the identification of a vortex, *J. Fluid Mech.*, **285**, 69-94.
- [14] Karamanos, G.S. and Karniadakis, G.E. (2000). A spectral vanishing viscosity method for large-eddy simulation, *J. Comput. Phys.*, **163**, 22-50.
- [15] Kravchenko, A.G. and Moin, P. (2000). Numerical studies of flow over a circular cylinder at  $Re=3900$ , *Phys. Fluids*, **12** (2), 403-417.
- [16] Lesieur, M. and Métais, O. (1996). New trends in large-eddy simulation of turbulence, *Annu. Rev. Fluid Mech.*, **28**, 45-82.
- [17] Maday, Y. et al. (1993). Legendre pseudo-spectral viscosity method for nonlinear conservation laws, *SIAM J. Numer. Anal.*, **30** (2), 321-342.
- [18] Maday, Y., et al. (1990). An operator-integration-factor splitting method for time-dependent problems: application to incompressible fluid flow, *J. of Sci. Comp.*, **5** (4), 263-292.
- [19] Pasquetti, R. and Xu, C.J. (2002). High-order algorithms for large eddy simulation of incompressible flows, *J. Sci. Comput.*, **17** (1-4), 273-284.
- [20] Phillips, R.M. and Phillips, T.N. (2000). Flow past a cylinder using a semi-Lagrangian spectral element method, *Appl. Num. Math.*, **33**, 251-257.
- [21] Sagaut, P. (1998), *Introduction à la simulation des grandes échelles pour les écoulements de fluide incompressible*, Mathématiques & Applications, Springer.
- [22] Stolz, S. and Adams, N.A. (1999). An approximate deconvolution procedure for large-eddy simulation, *Phys. Fluids*, **11** (7), 1699-1701.
- [23] Stolz, S. et al. (2001). An approximate deconvolution model for large-eddy simulation with application to incompressible wall-bounded flows, *Phys. Fluids*, **13** (4), 997-1015.
- [24] Tadmor, E. (1989). Convergence of spectral methods for nonlinear conservation laws, *SIAM J. Numer. Anal.*, **26** (1), 30-44.
- [25] Xu, C.J. and Pasquetti, R. (2001). On the efficiency of semi-implicit and semi-Lagrangian spectral methods for the calculation of incompressible flows, *Inter. J. Numer. Meth. Fluids*, **35**, 319-340.
- [26] Xu, C.J. and Pasquetti, R. (2003). Stabilized spectral element computations of high Reynolds number incompressible flows, *J. Comput. Phys.*, in press.